Pergamon

Int. J. Heat Mass Transfer. Vol. 38, No. 4, pp. 679–690, 1995

0017-9310/95 $9.50+0.00

0017-9310(94)00188-X

The interaction of an isolated sprinkler spray and a two-layer compartment fire environment

LEONARD Y. COOPER

National Institute of Standards and Technology, Gaithersburg, MD 02899, U.S.A.

(*Received* 2 *September* 1993 *and in final form* 13 *June* 1994)

Abstract—A model is developed to simulate the interaction of a sprinkler and a two-layer fire environment under arbitrary conditions of sprinkler elevation, upper- and lower-layer thickness, and temperature. The sprinkler is characterized by a water flow rate and four measurable device parameters. The model simulates the effects of the sprinkler spray as it entrains, drives downward, humidifies, and cools gases in the upper and lower layers. It predicts the flow rates of mass, enthalpy, products of combustion and evaporated water to each of the two layers as a result of sprinkler operation. Results of example calculations are presented.

SPRINKLER–LAYER INTERACTION PHENOMENA

Consider a compartment fire with an operating isolated sprinkler. Assume a two-layer-type description of the fire-generated environment, where the thickness of the layers, and the assumed-uniform layer properties are known. Figure 1 illustrates generic interactions between the fire environment and the sprinkler. The analysis to follow considers possible interactions in terms of three categories [Fig. 1(a)–(c)] involving six possible flow conditions (COND 1–6). In Fig. 1(a) and (b) the elevated-temperature upper layer submerges the sprinkler, whereas in Fig. 1(c) (COND 1) the layer interface is at or above the sprinkler.

In Fig. 1(a) and (b), the sprinkler entrains, drives downward (aerodynamic drag on the spray drops), humidifies and cools (drop evaporation) gases from the high temperature upper layer. A jet of downward-moving gases is formed. Consistent with experiments with a sprinkler in an ambient environment [1], the jet is assumed to be confined to a fixed and specified spray zone of influence, a spray cone envelope.

The jet penetrates the layer interface. There it is typically upward-buoyant because below the interface the jet gases are usually warmer and less dense than the relatively cool lower layer environment. The penetrating jet can also be cooler and more dense.

In the lower layer, upward buoyant forces would reduce the jet velocity. Also, downward drag and spray evaporation continue as in the upper layer, albeit with reduced intensity. Upward buoyant forces on the jet may or may not be strong enough to drive it back upward, returning it to the upper layer. If the jet *is not* driven back then it is deposited in the lower layer as in Fig. 1(b). If the jet *is* buoyed back upward it can entrain a very large flow of lower layer gases. These would also be deposited into the upper layer as in Fig. 1(a). The phenomenon could lead to a vigorous mixing of upper and lower layers that can be described as 'smoke-logging'. Let $\dot{M}$ be the mass flow rate of the jet gases through a section of the spray cone. As indicated in the captions, Fig. 1(a) and (b) conditions are determined on the basis of whether, immediately below the interface, $d\dot{M}/dx$ is $\leqslant$ or >0.

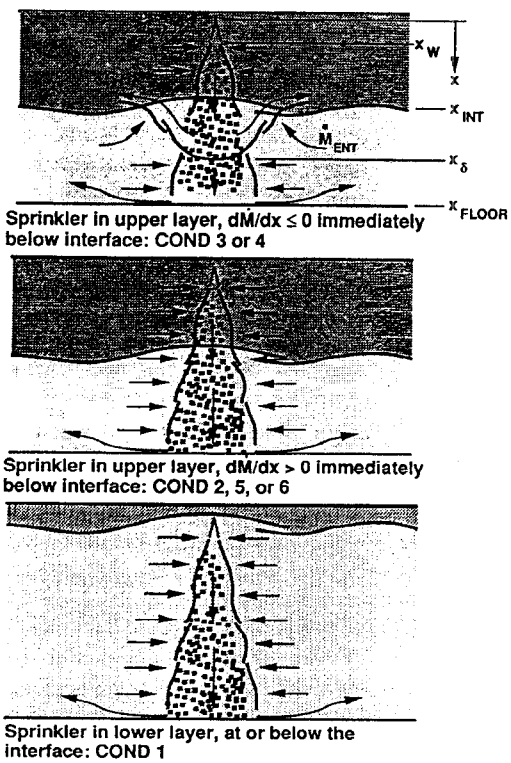

Fig. 1. The three generic scenarios for interaction of an operating sprinkler and a two-layer fire environment.

NOMENCLATURE

A_{SPRAY} cross-section area of the spray cone
B' mass transfer number
$c_{K,U}, c_{K,L}$ mass fraction of product K in upper, lower layer [(kg of product K)/(kg layer)]
C_D drag coefficient
C_M ratio of initial momentum of spray to momentum of water flow out of nozzle.
C_p specific heat of air at constant pressure at 293 K [1.004 kJ kg^{-1} K^{-1}]
D diameter of the spray cone
D_N, D_W diameter of sprinkler nozzle, spray at $x = x_w$
d volume-mean diameter of the spray drops
F_d drag force on a single drop
Fr Froude number, equation (39)
$f(\dot{M}^*)$ equation (26)
g acceleration of gravity [9.8 m s^{-2}]
h, h^* heat transfer coefficient, equation (10), dimensionless h, equation (26)
k thermal conductivity of air at the T_{REF}
L_W latent heat of vaporization of water [2.26 × 10^3 kJ kg^{-1}], ref. [5]
$\dot{m}_d$ mass rate of water evaporation from a single drop
$\dot{M}_U, \dot{M}_L$ net rate of mass flow to the upper, lower layer due to sprinkler operation
$\dot{M}_{ENT}$ mass rate of entrainment of reversed plume flow
$\dot{M}, \dot{M}^*$ mass rate of gases entrained into cone, dimensionless $\dot{M}$, equation (21)
$\dot{M}_d$ mass rate of water evaporation from all drops in spray cone
N number of drops per unit volume in spray cone
Nu hd/k
Pr Prantdl number of air
$\dot{P}_{K,U}, \dot{P}_{K,L}$ net rate of flow product K to upper, lower layer due to sprinkler operation
$\dot{Q}_U, \dot{Q}_L$ net rate of flow of enthalpy plus heat transfer to upper, lower layer
$\dot{q}_d$ rate of heat transfer to air from a single drop
$\dot{Q}_d, \dot{Q}_d^*$ rate of heat transfer from drops to gas, dimensionless $\dot{Q}_d$, equation (29)
Re, Re_M Reynolds numbers
r drop size parameter, equation (3)
$T, T_{REF}, \bar{T}$ temperature of air, reference T, average T in spray cone between x_{INT} and x_δ
$T_{1/3}$ characteristic T, equation (5)
T_U, T_L T of upper, lower layer
T_{LAYER} T of layer at the local elevation
T_p temperature of drop surface; wet bulb temperature corresponding to T_s
T_s, T_{s0} T in free stream of spray cone, $T_s(x = x_w)$
T^*_{SUB} T_{SUB}/T_{REF} for any subscript SUB
u, u_{EQ} velocity, equivalent u of air in spray cone between x_{INT} and x_δ
u_n nozzle discharge velocity
u_p, u_{p0} u of drops in spray cone, $u_p(x = x_w)$
u_{REL} $|u_p - u_s|$
u_s, u_{s0} u of air in spray cone, $u_s(x = x_w)$
u_p^*, u_s^* $u_p/u_{p0}, u_s/u_{p0}$
$\dot{V}_N$ volumetric water discharge rate of the nozzle
x distance below spray cone apex
x_{FLOOR}, x_{INT} x at: floor, layer interface, $y_{LAYER} - y_{FLOOR}$
x_M, x_w, x_δ x at: highest elevation where equation (32) is satisfied, break-up of sprinkler nozzle stream is complete, jet penetration depth
x^*_{SUB} x_{SUB}/D_W for any subscript SUB.

Greek symbols

β equation (31)
δ_p jet penetration depth, $x_\delta - x_{INT}$
ε arbitrarily small positive number
θ sprinkler spray angle
Λ_i equations (31)
λ_1, λ_2 equations (26)
$\mu, \mu_{1,3}, \mu_s$ dynamic viscosity of air, characteristic μ, equation (5), μ in free stream of spray cone
ν, ν_{REF} kinematic viscosity of air, $\nu(T_{REF} = 293\ K)$ [1.49 × 10^{-5} m^2 s^{-1}]
$\rho, \bar{\rho}, \rho_s$ density of air, $\rho(T = \bar{T})$, ρ in free stream of spray cone
ρ_{REF} $\rho(T = T_{REF})$ [1.2 kg m^{-3}]
ρ_W density of water [10^3 kg m^{-3}]
ρ_U, ρ_L density of upper, lower layer
σ equation (24)
ω_i $i = 1$ and 2, equation (24), $i = 3$ and 4, equation (25), $i = 6$, equation (26).

COND 4 and COND 3, depicted in Fig. 2, are associated with Fig. 1(a) when $x_\delta < x_{FLOOR}$ [Fig. 2(a)] and $x_\delta = x_{FLOOR}$ [Fig. 2(b)], respectively. COND 5 and COND 2, depicted in Fig. 3(a) and (b), respectively, and associated with Fig. 1(b), occur when $d\dot{M}/dx = 0$ at some $x \leqslant x_{FLOOR}$ in the lower layer (i.e. the jet stops entraining lower layer material and, with further increases in x, gas starts to be expelled from

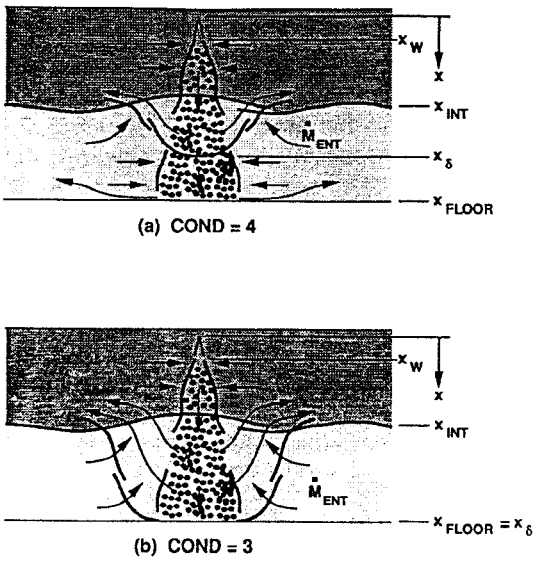

Fig. 2. Flow conditions of Fig. 1(a): COND 3 and 4.

the spray cone envelope). COND 5 and COND 2 are distinguished by $x_\delta < x_{FLOOR}$ [Fig. 3(a)] and $x_\delta = x_{FLOOR}$ [Fig. 3(b)], respectively. COND 6, depicted in Fig. 3(c) and also associated with Fig. 1(b), occurs when $d\dot{M}/dx > 0$ at all $x \leqslant x_{FLOOR}$ (i.e. the spray cone entrains material along its entire length). A complete qualitative description of the different flow conditions is presented in ref. [2].

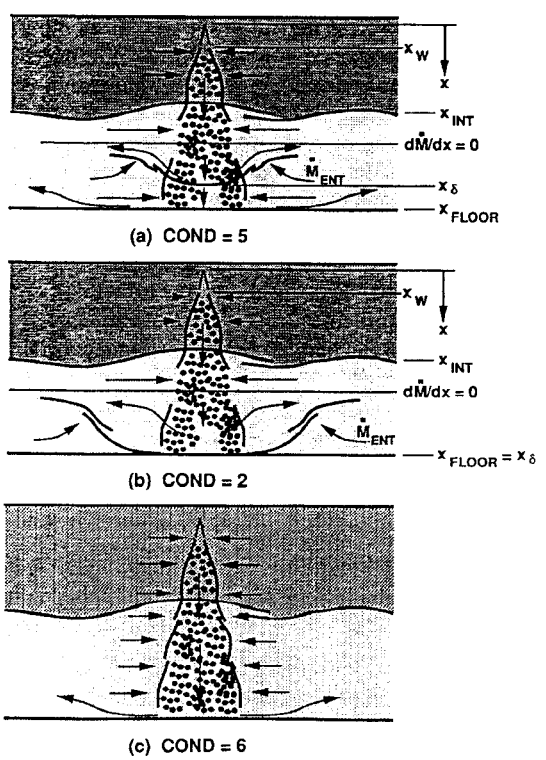

Fig. 3. Flow conditions of Fig. 1(b): COND 2, 5, or 6.

THE MODEL OF SPRINKLER–SMOKE-LAYER INTERACTION

The goal is a simulation of the interaction of sprinklers and two-layer fire environments, useable in zone-type fire models. This must predict the flow of mass, enthalpy, combustion products and evaporated water to each layer as a result of sprinkler operation.

Specifying the two-layer fire environment

The upper and lower layers have specified densities and temperatures ($\rho_U < \rho_L$, $T_U > T_L$) and specified mass fractions of water vapor and other products of combustion taken account of in the simulation. (Water is a product of both combustion and evaporation.) When implementing the simulation in a fire model, specification of layer product concentrations, including water concentration, would be required only when such concentrations are actually being predicted in the overall fire model simulation. Thus, the present sprinkler–layer interaction model *does not* depend on specification of the layer water concentrations. This is in spite of the fact that: (1) the model predicts, among other parameters, the rate of water evaporation and cooling from the sprinkler spray drops; and that (2) such evaporation is generally a function of the humidity of the gases entrained into the zone of influence of the water spray. The reason that water concentrations are not required is that the models used here for predicting evaporative cooling [3] and aerodynamic drag [4] of evaporating droplets are based on the assumption that the relative humidity of the gases in the spray envelope is negligible. In the present application this seems to be a reasonable assumption since most of the evaporative cooling is expected to occur at gas temperatures at least several tens of degrees K above ambient and at relatively early times, when the high mass fractions of water associated with high relative humidity are not expected.

FORMULATION OF THE PROBLEM FOR THE FLOWS IN THE SPRAY CONE ENVELOPE

Fragmentation of the nozzle flow—the spray cone envelope

Break-up of the sprinkler water stream into drops (e.g. fragmented by impingement with a striker plate, or by fluid-dynamic instabilities) is assumed to be complete at an elevation, x_w, relatively close to the sprinkler nozzle outlet. There the spray is assumed to be well-simulated as having a cone-like volume of influence, with cone angle θ, a characteristic of the sprinkler device. (Ref. [1] considers devices with θs from 30 to 120°.) The virtual apex of the cone is the origin of the x axis directed downward and coincident with the spray-cone axis. Corresponding to x and x_W are the spray-cone diameters D and D_W, respectively,

$$D = 2x \tan(\theta/2) \quad D_W = 2x_W \tan(\theta/2). \qquad (1)$$

The speed of the nozzle flow is:

$$u_N = \dot{V}_N/(\pi D_N^2/4) \quad (2)$$

where nozzle diameter and volumetric discharge rate are D_N and $\dot{V}_N$, respectively; D_N and either u_N or $\dot{V}_N$ are specified. Fragmentation of the nozzle stream is accompanied by a loss of downward momentum, this being a characteristic of the sprinkler device. C_M (representative value, 0.4 [1]) is the ratio of water spray momentum at x_w to that of the nozzle stream.

The drops of the water spray are modeled as spheres with diameters equal to the mean-volume diameter, d. Measurements for air–water spray–sprinkler systems indicate:

$$d = r(D_N/u_N)^{2/3} \quad (3)$$

where r is a drop-size parameter of the spray device (representative value, 0.084 m $s^{-2/3}$ [1]).

Drag forces between the drops and the jet gases

Downward drop velocity leads to a momentum transfer due to drag-force interactions between the drops and the gas. This results in a downward flow of the gas within the spray cone and relatively low pressure there (compared to pressures at large radii, outside the cone). The low pressures drive an entrainment of gases toward the spray cone axis from the relatively quiescent far-field. With increasing x, conservation of vertical momentum along the spray cone axis requires acceleration of the gas at the expense of deceleration of the drops. The result is a downward jet of upper layer gas in the spray cone envelope.

In the spray cone, differences in velocity and temperature of gas and drops lead to evaporative cooling. The drag on a water drop evaporating in air in the Reynolds number-range of interest, $10 < Re < 1000$, can be approximated by [1, 4]:

$$|F_d| = (1/2)\rho_s u_{REL}^2 C_D(\pi d^2/4) \quad C_D = 12.6/Re^{1/2} \quad (4)$$

$$Re = u_{REL}\, d\rho_s/\mu_{1/3} \quad \mu_{1/3} = \mu(T_{1/3})$$

$$T_{1/3} \equiv T_p + (T_s - T_p)/3. \quad (5)$$

Results of ref. [4] indicate that, in the Re range of interest, equation (4), with an equation-(5) calculation of Re based on $\mu_s = \mu(T_s)$ rather than $\mu_{1/3}$, will typically lead to a predicted value for C_D that is a several tens of per cent greater than the true value. It was this latter value of Re, based on μ_s, that was used in refs. [1] and [5] to compute F_d in equation (4).

For steady state, the evaporation process keeps the drop surface at the wet bulb temperature corresponding to T_s [4]. This is assumed to hold here. Ref. [5] provides the following approximation to $T_p(T_s)$ data of ref. [4] in the range 373 K $\leqslant T_s \leqslant$ 1273 K:

$$T_p = 266[1 + 3.23(10)^{-4} T_s\ \mathrm{K}^{-1}]. \quad (6)$$

As in ref. [5], it is assumed for air that:

$$\mu = \rho\nu \propto T^{0.7} \quad \rho T = \text{constant} \quad (7)$$

where, for reference temperature, $T_{REF} = 293$ K,

$$\rho_{REF} \equiv \rho(T_{REF}) = 1.2\ \mathrm{kg\,m^{-3}}$$

$$\nu_{REF} \equiv \nu(T_{REF}) = 1.49 \times 10^{-5}\ \mathrm{m^2\,s^{-1}}. \quad (8)$$

Defining T_s^* and using equations (6)–(8) in equation (5) leads to the following, for use in calculating F_d:

$$T_s^* = T_s/T_{REF}$$

$$Re = (u_{REL} d/\nu_{REF})/[0.518 T_s^*(T_s^* + 1.55)^{0.7}]. \quad (9)$$

Heat and mass transfer between the drops and the jet gases

For non-zero relative motion the rate of heat transfer to the air from a water drop is [3]:

$$\dot{q}_d = -h\pi d^2(T_s - T_p)$$

$$Nu = hd/k = [2 + 0.6 Re_M^{1/2} Pr^{1/3}]/(1 + B') \quad (10)$$

where $200 < Re_M < 2000$ and where all properties are evaluated at $(T_s + T_p)/2$ except for density in Re_M, which is taken to be ρ_s. Note that Re_M is different than Re.

Using equations (6)–(8) and a curve fit to $B'(T_s)$ data for water [3] (range 373 K $\leqslant T_s \leqslant$ 1273 K), ref. [5] provides the following version of equation (10) for air–water systems:

$$h[\mathrm{kW\,m^2\,K^{-1}}] = \{4.55(10^{-3}) T_s^{*-1/2}(T_s^* + 0.836)^{-2.5}$$

$$\times |u_p - u_s|[\mathrm{s\,m^{-1}}](d[\mathrm{m^{-1}}])^{1/2} + 5.16 \times 10^{-5}\}/$$

$$\{[1 + 0.100(T_s^* - 0.932)^{1.19}] T_s^{*-0.85} d[\mathrm{m^{-1}}]\} \quad (11)$$

where $T_s^* - 0.932 \neq 0$ since this corresponds to $T_s = 273$ K, outside equation (11)'s useful range.

Drop temperatures are assumed uniform at the local T_p (306 K $\leqslant T_p \leqslant$ 368 K for 373 K $\leqslant T_s \leqslant$ 1273 K [4]). Also, the rate of energy transfer to the drop required to maintain its changing T_p value is assumed negligible compared to the rate of heat transfer of equation (10). Thus, all heat transfer to the drops is used in the evaporation process. Finally, once the drops are formed near the nozzle, the total mass evaporated during their motion from x_w to x_{FLOOR} is assumed to be negligible compared to their original mass.

Using the first of equation (10), the rate of evaporation of water vapor from a drop is:

$$\dot{m}_d = -\dot{q}_d/L_w. \quad (12)$$

Problem variables and parameters

Quasi-steady conditions are assumed, where spray cone variables have 'top-hat' profiles and depend only on x; gas temperature, $T_s(x)$; and drop and gas velocities, $u_p(x)$, and $u_s(x)$:

$$T_{s0} \equiv T_s(x = x_w) \quad u_{p0} \equiv u_p(x = x_w)$$

$$u_{s0} \equiv u_s(x = x_w). \quad (13)$$

It is also assumed that:

$$T_{s0} = T_{LAYER} \quad u_{s0} = 0 \tag{14}$$

where T_{LAYER} is the layer temperature at x_w, T_L or T_U. Thus, air entrainment between the nozzle and x_w is assumed negligible. It is noteworthy that, in ref. [1], for sprays interacting with an ambient environment, calculated downstream values of u_s in the absence of evaporative cooling were shown to be insensitive to choice of u_{s0}.

From the definition of C_M and from conservation of mass flow rate of the water:

$$u_{p0} = C_M u_N \tag{15}$$

$$D_W = D_N / C_M^{1/2}. \tag{16}$$

Finally, define dimensionless variables:

$$u_p^* = u_p/u_{p0} \quad u_s^* = u_s/u_{p0} \quad T_{LAYER}^* = T_{LAYER}/T_{REF}$$
$$x^* = x/D_W = xC_M^{1/2}/D_N. \tag{17}$$

Conservation equations for the spray envelope

Conservation of mass for the drops—the drop number density. With specified $\dot{V}_N$ and d, conservation of water in the spray cone is invoked in terms of drop density. Equating volume flow rate of drops at any x to volume flow rate from the nozzle leads to:

$N \equiv$ number of drops per unit volume

$$= (3/2)u_N^2/[\pi r^3 D_N^2 \tan^2(\theta/2) u_p^* x^{*2}]. \tag{18}$$

Conservation of mass for the gas. Define:

$\dot{M} \equiv$ mass flow rate of layer gases entrained into spray cone from x_w to x. (19)

Since the mass of evaporated water is assumed to be negligible and since there is negligible gas flow in the spray cone at x_w, $\dot{M}$ is also the gas mass flow rate in the spray cone:

$$\dot{M} = \rho_s u_s A_{SPRAY} \quad A_{SPRAY} = \pi D^2/4. \tag{20}$$

Equations (19) and (20) are made dimensionless as follows:

$$\dot{M}^* \equiv \dot{M}/[4\rho_{REF}\dot{V}_N \tan^2(\theta/2)] \quad \dot{M}^* = u_s^* x^{*2}/T_s^*. \tag{21}$$

Below, it will be useful to calculate $d\dot{M}^*/dx^*$. Using equation (21), this will be obtained from:

$$d\dot{M}^*/dx^* = (x^{*2}/T_s^*)[du_s^*/dx^* + 2u_s^*/x^* - \sigma(u_s^*/T_s^*)\, dT_s^*/dx^*] \tag{22}$$

where the σ term is neglected in an analysis that involves the Boussinesq approximation.

$$\sigma = \begin{cases} 0 \text{ with the Boussinesq approximation} \\ 1 \text{ without the Boussinesq approximation.} \end{cases} \tag{23}$$

Once u_s^* and T_s^* are determined, $\dot{M}^*$ can be determined directly from equation (21).

Conservation of momentum for drops. Conservation of momentum of drops leads to:

$$du_p^*/dx^* = \omega_1/u_p^* - \omega_2(T_s^* + 1.55)^{0.35} \times (u_p^* - u_s^*)^{3/2}/(T_s^{*1/2} u_p^*)$$
$$\omega_1 = gD_N/(u_N^2 C_M^{5/2})$$
$$\omega_2 = 0.540B(v_{REF}U_N/r^3)^{1/2}(\rho_{REF}/\rho_W)/C_M. \tag{24}$$

On the right side of the first of equation (24), the terms represent the gravity (buoyancy) and drag forces on a drop, respectively, where the drag was determined from equations (4) and (9).

Equation (24) corresponds to equation (12) of ref. [1] or equation (1) of ref. [5], except for differences in the evaluation of Re discussed below equation (5). In ref. [5], which deals with the two-layer fire environment, equation (24) was only used in the upper layer. Here, equation (27) and all other conservation-derived equations, presented below, are used to simulate the dynamics in the spray cone in both the upper and lower layers for all scenarios of Figs. 1–3.

Conservation of momentum for gas. Conservation of momentum for the gas leads to:

$$du_s^*/dx^* = -u_s^*/x^* + \omega_3 T_s^{*1/2} \times (T_s^* + 1.55)^{0.35}(u_p^* - u_s^*)^{3/2}/(u_p^* u_s^* x^{*2}) + \omega_4(1 - T_s^*/T_{LAYER}^*)/u_s^* + \sigma[u_s^*/(2T_s^*)]\, dT_s^*/dx^*$$
$$\omega_3 = \omega_2(\rho_W/\rho_{REF})/[8\tan^2(\theta/2)]$$
$$\omega_4 = gD_N/(u_N^2 C_M^{3/2}) = C_M\omega_1. \tag{25}$$

On the right side of the first of equation (25), the second and third terms represent drag and buoyancy forces on the gas, respectively. The drag is equivalent to and in the opposite direction of the single-drop drag term of equation (24). The drag per unit volume on the gas was found by determining NF_d from equations (4) and (18). Equation (25), with $\sigma = \omega_4 = 0$, i.e. neglecting buoyancy, follows equation (2) of ref. [5], except for differences in Re, as discussed below equation (5).

Conservation of energy for gas. Conservation of energy for the gas leads to:

$$dT_s^*/dx^* = \{(T_s^*/u_s^*)/[1 + \sigma f(\dot{M}^*)]\} \times [f(\dot{M}^*)(du_s^*/dx^* + 2u_s^*/x^*) - \omega_5(T_s^* - 0.993) \times h^*(T_s^*, u_s^*, u_p^*; \lambda_1, \lambda_2)/(u_p^* x^{*2})]$$
$$h^* = [5.16\times10^{-5} + 4.55\times10^{-3}\lambda_1 T_s^{*-1.2} \times (T_s^* + 0.836)^{-2/5}|u_p^* - u_s^*|]/\{[1 + 0.100(T_s^* - 0.932)^{1.19}]\lambda_2 T_s^{*-0.85}\}$$
$$\omega_5 = 1.14[(D_N/r)/(4\dot{V}_N/\pi)^{1/3}][\text{m s}^{-1}]/[C_M \tan^2(\theta/2)]$$
$$\lambda_1 = [(4\dot{V}_N/\pi)^{2/3} r^{1/2}/D_N][\text{s m}^{-3/2}]$$
$$\lambda_2 = [D_N^2 r/(4\dot{V}_N/\pi)^{2/3}][\text{s}^{4/3}\text{ m}^{-5}]$$
$$f(\dot{M}^*) = \begin{cases} 0 & \text{if } d\dot{M}^*/dx^* \leqslant 0 \\ (T_{LAYER}^*/T_s^* - 1) & \text{if } d\dot{M}^*/dx^* > 0. \end{cases} \tag{26}$$

In the first of equation (26), heat transfer to the gas from the evaporating drops is represented by the term

with coefficient ω_5, which was found by determining $N\dot{q}_d$ from equations (10) and (18). The term $(du_s^*/dx^* + 2u_s^*/x^*)$ with the coefficient $f(\dot{M}^*)$, represents contributions to dT_s^*/dx^* due to air entrained into the jet gases from the far field at $T_{LAYER} \neq T_s$. From the form of $f(\dot{M}^*)$, it is seen that this term can lead to a non-zero contribution only at x^*s where the entrainment rate is positive, i.e. $d\dot{M}^*/dx^* > 0$. Where there is lateral outflow from the jet, e.g. immediately below the interface in Fig. 1(a), $d\dot{M}^*/dx^* \leqslant 0$, and $f(\dot{M}^*) = 0$. Thus, for this case equation (26) is seen to correctly predict that the terms in question do not directly affect dT_s^*/dx^*.

In deriving equations (26), $(T_s^* - T_p^*)$ was found from equation (6) to be:

$$(T_s^* - T_p^*) = 0.914(T_s^* - 0.993). \tag{27}$$

In the first of equation (26), this explains the appearance of the $(T_s^* - 0.993)$ coefficient of h^*.

Heat transfer and evaporation from drops. From equations (10) and (18) the total rate of heat transfer to the gas from the drops, from x_w to x, is computed from:

$\dot{Q}_d \equiv$ rate of heat transfer from drops to gas

$$= \int_{x_w}^{x} N\dot{q}_d A_{SPRAY}\, dx. \tag{28}$$

Dimensionless $\dot{Q}_d$ is defined and used in equation (28):

$$\dot{Q}_d^* \equiv \{C_M^{1/2}/[\pi D_N^2 \tan^2(\theta/2)\rho_{REF} C_p T_{REF} u_n]\}\dot{Q}_d$$

$$d\dot{Q}_d^*/dx^* = -\omega_5(T_s^* - 0.993)h^*(T_s^*, u_s^*, u_p^*; \lambda_1, \lambda_2)/u_p^*. \tag{29}$$

This is the heat transfer term of equation (26). Equation (29) properly indicates that $d\dot{Q}_d^*/dx^*$ is negative.

Consistent with equation (12), define and evaluate:

$$\dot{M}_d = -\dot{Q}_d/L_w$$

$$\equiv \textit{total rate of water evaporation from } x_w \text{ to } x. \tag{30}$$

The equation set for u_p^*, u_s^*, T_s^*, $\dot{Q}_d^*$, $\dot{M}^*$, *and* $\dot{M}_d$

Equations (24)–(26) are an independent, coupled set for du_p^*/dx^*, du_s^*/dx^*, and dT_s^*/dx^*. Because of the form of $f(\dot{M}^*)$ of equation (26), this appears to depend generally on *a priori* knowledge of the sign of $d\dot{M}^*/dx^*$, which, as seen in equation (22), is itself a function of du_s^*/dx^* and dT_s^*/dx^*. However, an analysis of the implications of assumptions on the sign of $d\dot{M}^*/dx^*$ reveals that the problem of determining $u_p^*, u_s^*, T_s^*, \dot{Q}_d^*, \dot{M}^*$, and $\dot{M}_d$ as functions of x^* can be presented as follows. Define:

$$\beta \equiv (T_{LAYER}^*/T_s^* - 1) = (1 - T_s^*/T_{LAYER}^*)/(T_s^*/T_{LAYER}^*)$$

$$\Lambda_1 \equiv \omega_1/u_p^*$$

$$\Lambda_2 \equiv \omega_2(T_s^* + 1.55)^{0.35}(u_p^* - u_s^*)^{3/2}/(T_s^{*1/2}u_p^*)$$

$$\Lambda_3 \equiv \omega_3 T_s^{*1/2}(T_s^* + 1.55)^{0.35}(u_p^* - u_s^*)^{3/2}/(u_p^* u_s^* x^{*2})$$

$$= (\omega_3/\omega_2)\Lambda_2 T_s^*/(u_s^* x^{*2})$$

$$\Lambda_4 \equiv \omega_4[\beta/(1+\beta)]/u_s^*$$

$$\Lambda_5 \equiv \omega_5(T_s^* - 0.993)\, h^*(T_s^*, u_s^*, u_p^*; \lambda_1, \lambda_2)/(u_p^* x^{*2}) \tag{31}$$

where $\omega_1, \omega_2, \omega_3, \omega_4, \omega_5$, and h^* are given in equations (25) and (26). Then:

if $\beta \leqslant 0$ and $[u_s^*/x^* + \Lambda_3 + \Lambda_4 + (\sigma/2)\Lambda_5] \leqslant 0$: (32)

$$du_s^*/dx^* = -u_s^*/x^* + \Lambda_3 + \Lambda_4 - (\sigma/2)\Lambda_5$$

$$dT_s^*/dx^* = -(T_s^*/u_p^*)\Lambda_5 \tag{33}$$

else, when equation (32) is not satisfied:

$$du_s^*/dx^* = [-(1-\sigma\beta)u_s^*/x^* + (1+\sigma\beta)(\Lambda_3 + \Lambda_4) - (\sigma/2)\Lambda_5]/[1 + (\sigma/2)\beta]$$

$$dT_s^*/dx^* = [\beta(u_s^*/x^* + \Lambda_3 + \Lambda_4) - \Lambda_5](T_s^*/u_p^*)/[1 + (\sigma/2)\beta] \tag{34}$$

whether or not equation (32) is satisfied:

$$du_p^*/dx^* = \Lambda_1 - \Lambda_2 \quad d\dot{Q}_d^*/dx^* = -\Lambda_5 x^{*2}$$

$$\dot{M}^* = \text{equation (21)} \quad \dot{M}_d = \text{equation (30)} \tag{35}$$

where, depending on whether or not a Boussinesq approximation is adopted, σ is given in equation (23). From equation (22) and the above results it follows that:

when equation (32) is satisfied:

$$d\dot{M}^*/dx^* = (x^{*2}/T_s^*)[u_s^*/x^* + \Lambda_3 + \Lambda_4 + (\sigma/2)\Lambda_5] \leqslant 0 \tag{36}$$

when (32) is not satisfied:

$$d\dot{M}^*/dx^* = (x^{*2}/T_s^*)[u_s^*/x^* + \Lambda_3 + \Lambda_4 + (\sigma/2)\Lambda_5]/[1 + (\sigma/2)\beta] > 0. \tag{37}$$

Elevations where equation (32) is satisfied correspond to elevations below the interface (since $\beta \leqslant 1$ means that $T_{LAYER}^* \leqslant T_s^*$) where there is outflow from the spray cone (since $d\dot{M}^*/dx^* \leqslant 0$).

For COND 1 and 6 flow conditions there is entrainment into the spray cone (i.e. $d\dot{M}^*/dx^* > 0$) along its entire length and equation (32) is never satisfied. For COND 3–5, there is always a portion of the length of the lower layer spray cone where equation (32) will be satisfied. Finally, for COND 2, equation (37) may or may not be satisfied in an elevation interval of the lower layer.

The problem solution is obtained by integrating equations (32)–(35) for $u_p^*, \dot{Q}_d^*, u_s^*$, and T_s^*, and then using equations (21) and (30) to determine $\dot{M}^*$ and $\dot{M}_d$. Initial conditions are:

$$\text{at } x^* = x_w^*: \quad u_p^* = 1 \quad \dot{Q}_d^* = 0 \quad u_s^* = 0 \quad T_s^* = T_{LAYER}^*. \tag{38}$$

Solving the problem for the spray cone envelope

A procedure for solving the problem in the spray cone is presented in the Appendix.

LOWER LAYER ENTRAINMENT RATE FROM x_{INT}^* TO x_σ^* IN FIG. 1(a) SCENARIOS

Jets and plumes with reversed, purely-buoyant body forces

Consider a fluid jet or plume of one density penetrating a fluid layer with a different density, ρ_L, where buoyant forces on the jet or plume fluid in the penetrated layer opposes its motion. Different aspects of this problem were studied experimentally in refs. [7] [Fig. 4(a)] and [8] [Fig. 4(b)] where the fluids were fresh water and salt water.

The result in ref. [7] was an estimate for δ_p, the penetration depth into the layer of the original 'top-hat-profile' jet used in the experiments. Define Froude number, Fr, as in ref. [7]:

$$Fr = u/[g(|\rho_L - \rho|/\rho)\, D/2]^{1/2}, \tag{39}$$

where u, D, and ρ are the velocity, diameter, and density, respectively, of the jet at penetration. From ref. [7], δ_p is obtained from:

$$2\delta_p/D = \begin{cases} 0 & \text{if } Fr \leqslant 1.1 \\ 3.69(Fr-1.1)^{0.87} & \text{if } Fr > 1.1. \end{cases} \tag{40}$$

The above estimate, an approximation of the data of ref. [7], is from ref. [5]. It highlights the result, consistent with observations in ref. [8], that δ_p/D is negligible for Fr less than approximately 1.

For tests with the configuration of Fig. 3(a), it was found in ref. [8] that $\dot{M}_{ENT}$, the rate of mass entrained by the reversed plume flow from the layer into which the plume is penetrating, is

$$4\dot{M}_{ENT}/[\rho_L D^2 u] = 2.44(\rho/\rho_L)^{1/2} Fr^3. \tag{41}$$

Equation (41) is from ref. [5]. It is a revised version of the original result of ref. [8]. It is based on the assumptions that: (1) at interface penetration the plume has identical dimensionless Gaussian velocity and density-defect profiles; and (2) $\dot{M}_{ENT}$ is identical to the entrainment from a penetrating 'top-hat-profile' jet with the same mass, momentum, and buoyancy fluxes.

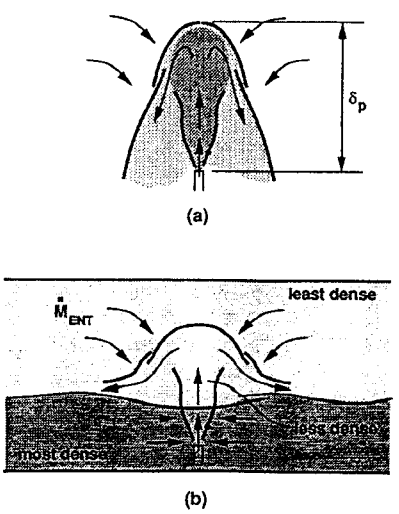

Fig. 4. Experimental studies of jets and plumes with reversed, purely buoyant body forces: (a) to determine δ_p [7]; and (b) to determine $\dot{M}_{ENT}$ [8].

Using the purely-buoyant-flow results to predict $\dot{M}_{ENT}$ of the Fig. 1(a) scenario

The flow dynamics of refs. [7] and [8] are very similar to the flow dynamics in the lower layer of a COND 3 or 4 scenario. However, there are important differences that should be taken account of if one is to adopt for present use the results of equations (40) and (41).

In equations (40) and (41), ρ is the average density of the jet at the elevation of interface penetration. However, in the present situation, prior to any entrainment from the lower layer environment, the density of the jet gases that penetrate the interface is altered from its value at the interface, $\rho_s(x = x_{INT})$. This is by virtue of a distributed volumetric heat sink (i.e. the evaporative cooling) between the interface and the penetration depth. To use equations (40) and (41) here, it is therefore evident that an equivalent jet penetration density other than $\rho_s(x = x_{INT})$, should be used for ρ. It is reasonable to choose this equivalent density to be $\bar{\rho}$, the density associated with the average temperature of the gases in the upward-buoyancy spray cone, $\bar{T}$, before any mixing with the entrained lower-layer gases.

Equation (40) and (41) are for a jet with penetration velocity u at the interface elevation and with only the gravitational body force (i.e. buoyancy) retarding and changing the direction of jet gas motion between the interface and the penetration depth. Considered here is a jet with penetration velocity $u_s(x = x_{INT})$, where, in addition to a retarding gravitational force, there is a volumetric drop-drag force acting to enhance rather than retard the downward jet gas velocity between the interface and the penetration depth. There is also the additional effect on the u_s distribution of contraction of the jet gases due to evaporative cooling. To use equations (40) and (41) here, it is therefore evident that an equivalent jet penetration velocity other than $u_s(x = x_{INT})$, should be used for u. This velocity is designated as u_{EQ}.

In view of equation (39) and the above discussion, Fr is computed from:

$$Fr = u_{EQ}/[g(\bar{T}/T_L - 1)D_{INT}/2]^{1/2}$$

$$D_{INT} \equiv D(x = x_{INT}) = 2x_{INT} \tan(\theta/2). \tag{42}$$

With a non-zero value of δ_p, computed with the

methods of previous sections, now use equation (40) to solve for Fr. Then use this in equation (39) to find u_{EQ}:

$$u_{EQ} = [g(\bar{T}/T_L - 1)D_{INT}/2]^{1/2} Fr$$

$$Fr = 1.1 + 0.223(2\delta_p/D_{INT})^{1.15} \quad (43)$$

[if the previous calculation indicates COND 3, where the upward buoyant jet in the lower layer impinges on the floor, then δ_p in equation (43) should be replaced by $(x_{FLOOR} - x_{INT})$].

Replacing u and ρ by u_{EQ} and $\bar{\rho}$, respectively, in equation (41) and using equation (43) leads to:

$$\dot{M}_{ENT} = 2.44\rho_{REF}(T_{REF}/T_L) \times [g(\bar{T}/T_L - 1)(D_{INT}/2)^5]^{1/2} Fr^4 \quad (44)$$

where Fr is computed from equation (43).

From the definition of $\bar{\rho}$, it follows that:

$$\bar{T} = T_U + \dot{Q}_d^*(x^* = x_\delta^* \text{ or } x_{FLOOR}^*)/[C_p \dot{M}^*(x^* = x_{INT}^*)] \quad (45)$$

where $\dot{Q}_d^*(x^* = x_\delta^*$ or $x_{FLOOR}^*)$ and $\dot{M}^*(x^* = x_{INT}^*)$ were obtained previously. Using equation (45) in equation (44) finally leads to the desired result for $\dot{M}_{ENT}$.

THE RATES OF FLOW OF MASS, ENTHALPY, AND PRODUCTS TO THE LAYERS

Assume that equation (31)–(38) have been solved for $u_p^*, u_s^*, T_s^*, \dot{Q}_d^*, \dot{M}^*$, and $\dot{M}_d$ in $x_w^* \leqslant x^* \leqslant x_{FLOOR}^*$. These results would then be used to obtain net rates of flow of mass, enthalpy, and arbitrary product K to the upper and lower layers, designated as $\dot{M}_U$, $\dot{M}_L$, $\dot{Q}_U$, $\dot{Q}_L$, $\dot{P}_{K,U}$, $\dot{P}_{K,L}$, respectively. Here the flow rates are calculated for each possible scenario of Fig. 1.

COND 3 or 4 scenarios

For COND 3 or 4 all mass, enthalpy, and products entrained by the spray cone in the upper layer and all water evaporated in the entire spray cone and its associated enthalpy is returned to the upper layer. This is convected via the upward-moving upward-buoyant flow that surrounds the spray cone in the elevation-interval $x_{INT}^* \leqslant x^* \leqslant x_\delta^*$ (or in $x_{INT}^* \leqslant x^* \leqslant x_{FLOOR}^*$ if there is no $x_\delta^* < x_{FLOOR}^*$). Compute $\dot{M}_{ENT}$ from equations (43)–(45). Then:

$$\dot{M}_U = \dot{M}_{ENT} - \dot{Q}_d(x^* = x_\delta^* \text{ or } x_{FLOOR}^*)/L_W$$

$$\dot{M}_L = -\dot{M}_{ENT} - [\dot{Q}_d(x_{FLOOR}^*) - \dot{Q}_d(x_\delta^*)]/L_W$$

$$\dot{P}_{H_2O,U} = \dot{M}_{ENT} c_{H_2O,L} - \dot{Q}_d(x^* = x_\delta^* \text{ or } x_{FLOOR}^*)/L_W$$

$$\dot{P}_{H_2O,L} = -\dot{M}_{ENT} c_{H_2O,L} - [\dot{Q}_d(x_{FLOOR}^*) - \dot{Q}_d(x_\delta^*)]/L_W$$

$$\dot{P}_{K,U} = \dot{M}_{ENT} c_{K,L}, K \text{ not } H_2O$$

$$\dot{P}_{K,L} = -\dot{M}_{ENT} c_{K,L} = -\dot{P}_{K,U}, K \text{ not } H_2O$$

$$\dot{Q}_L = -\dot{M}_{ENT} C_p T_L + [\dot{Q}_d(x_{FLOOR}^*) - \dot{Q}_d(x_\delta^*)]$$

$$\dot{Q}_U = \dot{M}_{ENT} C_p T_L + \dot{Q}_d(x^* = x_\delta^* \text{ or } x_{FLOOR}^*). \quad (46)$$

COND 2, 5, or 6 scenarios

For COND 2, 5, or 6 all mass, enthalpy, and products entrained by the spray cone in the upper layer are deposited into the lower layer. Also deposited in the lower layer is all water evaporated in the spray cone and its associated enthalpy. Per Fig. 3, all of these are introduced at the floor elevation where the spray jet gases impinge on the floor surface:

$$\dot{M}_U = -\dot{M}(x_{INT}^*)$$

$$\dot{M}_L = \dot{M}(x_{INT}^*) - \dot{Q}_d(x_{FLOOR}^*)/L_W$$

$$\dot{P}_{H_2O,U} = -\dot{M}(x_{INT}^*) c_{H_2O,U}$$

$$\dot{P}_{H_2O,L} = \dot{M}(x_{INT}^*) c_{H_2O,U} - \dot{Q}_d(x_{FLOOR}^*)/L_W$$

$$\dot{P}_{K,U} = -\dot{M}(x_{INT}^*) c_{K,U}, K \text{ not } H_2O$$

$$\dot{P}_{K,L} = \dot{M}(x_{INT}^*) c_{K,U} = -\dot{P}_{K,U}, K \text{ not } H_2O$$

$$\dot{Q}_L = \dot{M}(x_{INT}^*) C_p T_U + \dot{Q}_d(x_{FLOOR}^*)$$

$$\dot{Q}_U = -\dot{M}(x_{INT}^*) C_p T_U. \quad (47)$$

COND 1 scenario

For COND 1 the spray cone dynamics have no effect on the upper layer. All mass, enthalpy, and products entrained by the spray cone from the lower layer and all water evaporated in the spray cone and its associated enthalpy are deposited back into the lower layer at the floor elevation where the spray jet gases impinge on the floor surface:

$$\dot{M}_U = \dot{Q}_U = 0 \quad \dot{M}_L = -\dot{Q}_d(x_{FLOOR}^*)/L_W$$

$$\dot{P}_{H_2O,L} = -\dot{Q}_d(x_{FLOOR}^*)/L_W \quad \dot{P}_{K,U} = 0 \text{ for all } K$$

$$\dot{P}_{K,L} = 0, K \text{ not } H_2O \quad \dot{Q}_L = \dot{Q}_d(x_{FLOOR}^*). \quad (48)$$

EXAMPLE CALCULATIONS

Comparisons of calculations and experiments for a spray in an ambient environment

For a spray in a uniform, ambient-temperature environment the present model equations are almost identical to those of refs. [1, 5]. To verify the expected correspondence between calculated results of the two models, the present solution procedure was carried out for selected conditions identical to those indicated in the first row of Table 2 of ref. [1] or Tables 1 and 2 of ref. [5]. (In the nomenclature of refs. [1, 5] the conditions are: $\tau = 34.45$, i.e. $2\theta = 120°$; $\beta = 0.01$; and $\xi = 0.00075$.) Calculations with the present model essentially reproduced the corresponding results of refs. [1, 5]. As expected, this was in spite of the previously discussed difference in u_s initial conditions used in the two models. The present model also successfully simulated spray-induced jet volume flow rates, measured in ref. [5], at 1.52, 3.04 and 5.42 m,

below a Rockwood T-4 spray nozzle† in an ambient environment.

Interactions between fire environments and a Rockwood T-4 spray nozzle flow

This section presents results of using the present model to simulate the interactions of a sprinkler and a two-layer fire environment. The scenarios simulate operation of the Rockwood T-4 spray nozzle used in ref. [1]. Like automatic sprinklers used for fire protection, this device generates a spray by employing a deflector to intercept and fragment a solid water jet flowing from the nozzle [1]. The calculations simulate the effects of the sprinkler discharging near the top of the hot upper layer of conjectured two-layer fire environments.

The Rockwood T-4 spray nozzle has the following characteristics [1]:

$$C_M = 0.41 \quad r = 0.096\,\mathrm{m\,s^{-2.3}} \quad D_N = 0.00635\,\mathrm{m}. \tag{49}$$

For the test of ref. [1] with the highest nozzle pressure, the flow rate was 0.00107 $m^3 s^{-1}$ and the spray envelope had a diameter of 2.0, 2.7, and 3.1 m at 1.52, 3.04, and 5.78 m below the nozzle, respectively. Based on this, the spray envelope for all of these elevations is simulated by a 45° cone angle. The following operating condition are adopted for all calculations

$$\theta = 45^\circ \quad \dot{V}_N = 0.00107\,\mathrm{m^3\,s^{-1}}. \tag{50}$$

For all calculations it is assumed that $T_L = T_{REF}$ and that the apex of the spray cone is at the nozzle exit located 10 m above the floor. Two sets of calculations are carried out. In the first the upper-layer temperature is fixed and the layer interface elevation varies between that of the nozzle and the floor. In the second calculations, interface elevation is fixed and the upper-layer temperature is varied over a wide range.

The spray nozzle in a 600 K upper layer. The model was used to simulate the interaction of the spray and a two-layer fire environment with $T_U = 600$ K. $\dot{M}_{ENT}$ and x_δ are plotted in Fig. 5(a) as functions of x_{INT}. The COND numbers are also indicated in Fig. 5(a).

$x_{INT} = 0$ corresponds to a fire scenario where the interface is at the elevation of the spray nozzle. This leads to COND 1 with no effect on the upper layer.

For $0 < x_{INT} \leqslant 1.0$ m, COND 2 is predicted. As in Fig. 3, in spite of spray cone outflow in the lower portion of the lower layer, there is still upward buoyant gas in the cone as it impinges on the floor, i.e. $x_\delta = 10$ m. However, because of a computed 'shielding' inflow immediately below the interface, lower-layer mass entrained into the outer plume-like lower-layer flow does not return to the upper layer, i.e. $\dot{M}_{ENT} = 0$.

† The use of trade names is for descriptive purposes only, and should not be construed as endorsement by the National Institute of Standards and Technology.

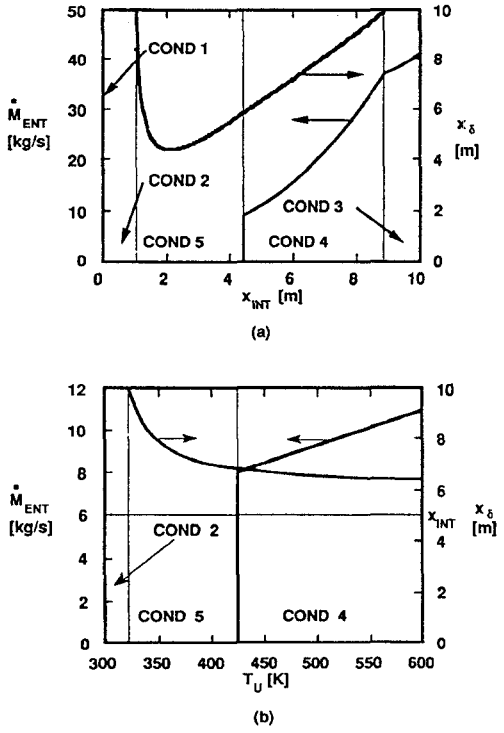

Fig. 5. Predictions of $\dot{M}_{ENT}$ and x_δ vs interface elevation for a spray nozzle operating in a two-layer fire environment: (a) a 600 K, variable-thickness, upper layer and a 293 K lower layer; and (b) a 5 m thick, variable-temperature upper layer and a 293 K lower layer.

For 1.0 m $< x_{INT} <$ 4.3 m the model predicts COND 5 (see Fig. 3). As with COND 2, because of a 'shielding' inflow, all flow penetrating the interface is mixed into the lower layer and, again, $\dot{M}_{ENT} = 0$. However, for this x_{INT} range none of the upward buoyant gases in the spray cone penetrate to the floor, i.e. $x_\delta < 10$ m.

At $x_{INT} = 4.3$ m the model predicts a discontinuity in $\dot{M}_{ENT}$ and for 4.3 m $< x_{INT} \leqslant 8.9$ m COND 4 is predicted (see Fig. 2). All upward buoyant flow in the lower layer, involving a relatively large entrained flow rate ranging from $\dot{M}_{ENT} = 8$ to 37 kg s^{-1}, is predicted to return to the upper layer. Thus, an abrupt and relatively massive growth rate of the upper layer would be predicted as the upper-layer thickness grows beyond 4.3 m.

For 8.9 m $< x_{INT} <$ 10 m the model predicts COND 3 (see Fig. 2) where all penetrating flow and all flow entrained from the lower layer returns to the upper layer. Here $\dot{M}_{ENT}$ continues to increase with increasing upper-layer thickness. In this range, upward buoyant plume gases in the spray cone once again impinge on the floor with $x_\delta = 10$ m.

The nozzle spray penetrating a 5 m upper layer. The model was also used to simulate the interaction of the spray and a two-layer fire environment with a 5 m upper layer thickness, with T_U in the range 300 K $\leqslant T_U \leqslant$ 600 K. $\dot{M}_{ENT}$ and x_δ are plotted in Fig.

5(b) as functions of T_U and the corresponding COND numbers are indicated.

For 300 K $\leqslant T_U <$ 425 K, COND 2 or 3 are seen to prevail and none of the upward buoyant flow entrainment in the lower layer is returned to the upper layer, i.e. $\dot{M}_{ENT} = 0$. As T_U increases beyond 425 K, the situation changes abruptly as upward buoyant flow in the lower layer is able to enter the upper layer. As seen in the figure, when T_U goes beyond this 'threshold' temperature a significant flow rate, $\dot{M}_{ENT} = 8$ kg s^{-1}, of entrained lower-layer gas is predicted to be deposited into the upper layer. As T_U rises from 425 to 600 K, $\dot{M}_{ENT}$ increases to approximately 11 kg s^{-1} and the flow condition remains at COND 4.

Summary of calculations; ceiling venting to enhance sprinkler effectiveness

The above example calculations illustrate some of the important effects of the interaction of a sprinkler spray and a two-layer fire environment. The phenomenon highlighted by the calculations is the abrupt and large change in sprinkler–layer interaction that comes about as an upper layer increases in thickness beyond a critical thickness (for a given upper-layer temperature) or increases in upper-layer temperature beyond a critical temperature (for a given upper-layer thickness). When the layer does not exceed the critical values the sprinkler spray is predicted to have a relatively small effect on the upper layer. In particular, the model predicts that the spray simply entrains and extracts a relatively small flow of upper gases and deposits it into the lower layer. When the critical values are exceeded, the model predicts that a very large rate of relatively cool lower-layer gases, up to the order of 10 kg s^{-1} in the example calculations, is entrained and transferred to the upper layer. This would be accompanied by a redeposition into the upper layer of all of those upper-layer gases, cooled and humidified by spray drop evaporation, which are continuously extracted from the upper layer by the action of the spray cone entrainment there.

The net result of the above predicted sprinkler–layer interaction would be a very large rate of growth in the thickness of the upper layer, a growth that in practice could lead to rapid and complete smoke filling of even the largest compartments of fire origin.

From the above results and discussion, it would appear that control or delay of the temperature and/or thickness of the upper layer to below-critical levels would lead to predictable design-response sprinkler–fire interactions, i.e. sprinkler–fire interactions which do not significantly deviate from design conditions. For example, it is possible that the relatively prompt use of ceiling venting could provide the suggested desirable smoke layer control. Indeed, use of ceiling venting to provide such control, without significant smoke logging, could be the basis of a strategy of coordinated sprinkler–vent design leading to effective fire control/suppression in compartments of fire origin.

USING THE SPRINKLER–LAYER INTERACTION MODEL IN LAVENT [9, 10]

The full implications of the sprinkler–layer model developed here can only be assessed within the context of simulations involving a complete compartment fire model. One likely candidate model is the two-layer zone compartment fire model computer code LAVENT (Link Actuated VENTs) [9–11]. LAVENT simulates the development of the fire environment in a compartment of fire origin outfitted with fusible-link-actuated ceiling vents and sprinklers. LAVENT simulates the environment in the fire compartment up to the time that the first sprinkler link fuses and the water flow from the actuated sprinkler nozzle is initiated.

By including the present sprinkler–layer interaction model in LAVENT, the revised compartment fire model would be able to simulate the fire environment beyond the time of first sprinkler operation, including the effects of subsequent actuation of additional ceiling vents and/or sprinkler nozzle flows.

SUMMARY AND CONCLUSIONS

A mathematical model was developed to simulate the interaction of an isolated operating sprinkler and a two-layer fire environment under arbitrary conditions of sprinkler-nozzle elevation, upper- and lower-layer thickness, and temperature. The sprinkler is characterized by water flow rate, nozzle diameter, and three other measurable device parameters related to: the drop size of the water flow after fragmentation of the nozzle flow stream; the momentum of the stream after fragmentation; and an effective cone angle of the sprinkler spray. The model takes account of all effects of the sprinkler spray as it entrains, drives downward, humidifies, and cools gases from both the high temperature upper layer and the relatively cooler lower layer.

A specific objective of the model was to provide a means of predicting the rates of flow of mass, enthalpy, products of combustion, and evaporated water to each of the two layers as a result of sprinkler operation. An algorithm for such predictions, suitable for general use in two-layer zone-type compartment fire models, was presented.

The model was exercised in example calculations which simulate the interaction between the spray of a real sprinkler device and both fire and non-fire environments. Limited validation of the model was achieved in the simulation of experiments involving the operation of a spray nozzle flow operating in a uniform, ambient-temperature, non-fire environment [1, 5]. Model validation in experiments involving sprinklers in fire environments is required.

Example calculations simulated the interaction of

an operating Rockwood T-4 spray nozzle and a variety of two-layer fire environments in a 10 m high space. An important generic phenomenon identified in these calculations was the abrupt and large change in sprinkler–layer interaction that comes about as an upper layer increases in thickness beyond a critical thickness (for a given upper-layer temperature) or increases in upper-layer temperature beyond a critical temperature (for a given upper-layer thickness). When the layer does not exceed the critical values, the sprinkler spray is predicted to result in relatively little mixing between the layers. However, when the critical values are exceeded the model predicts that a very large flow of lower-layer gases is transferred to the upper layer by entrainment into the upward buoyant flow that is driven out of the upper layer by direct action of the water spray. The net result of the latter predicted sprinkler–layer interaction would be a very large rate of growth in the thickness of the upper layer, a growth that could lead to rapid and complete smoke filling of even the largest compartments of fire origin.

The above calculation results suggested that control or delay of the temperature and thickness of the upper layer to below-critical levels could be useful in guaranteeing sprinkler–fire interactions, without smoke logging (smoke filling of the entire space), which do not significantly deviate from design conditions. It is possible that the relatively prompt use of ceiling venting could provide the suggested desirable smoke layer control.

The model should be assessed in the context of a full compartment fire model simulation.

Acknowledgement—The author acknowledges gratefully the American Architectural Manufacturers Association (AAMA) Research Foundation which supported this work.

REFERENCES

1. G. Heskestad, H.-C. Kung and N. F. Todenkopf, Air entrainment into water sprays, Technical Report RC-77-TP-7, Factory Mutual Research Corporation, Norwood, MA (November 1977).
2. L. Y. Cooper, Interaction of an isolated sprinkler spray and a two-layer compartment fire scenario, NISTIR 4587, National Institute of Standards and Technology, Gaithersburg, MD (1991).
3. M. C. Yuen and L. W. Chen, Heat transfer measurements of evaporating liquid droplets, *Int. J. Heat Mass Transfer* **21**, 537–542 (1978).
4. M. C. Yuen and L. W. Chen, On drag of evaporating liquid droplets, *Comb. Sci. Technol.* **14**, 147–154 (1976).
5. G. H. Heskestad, Sprinkler/hot layer interaction. Technical Report FMRC J. I. OT1N2.RU, Factory Mutual Research Corporation, Norwood, MA (September 1990).
6. J. H. Keenan and J. Kaye, *Gas Tables*. Wiley (1957).
7. J. S. Turner, Jets and plumes with negative or reserving buoyancy, *J. Fluid Mech.* **26**, 779–792 (1966).
8. W. D. Baines, Entrainment by a plume or jet at a density interface, *J. Fluid Mech.* **68**, 309–320 (1975).
9. L. Y. Cooper, Estimating the environment and the response of sprinkler links in compartment fires with draft curtains and fusible link-actuated ceiling vents: theory, *Fire Safety J.* **16**, 137–163 (1990).
10. W. D. Davis and L. Y. Cooper, Estimating the environment and the response of sprinkler links in compartment fires with draft curtains and fusible link-actuated ceiling vents—Part II: user guide for the computer code LAVENT, NISTIR 89-4122, National Institute of Standards and Technology, Gaithersburg, MD (August 1989).
11. W. D. Davis and L. Y. Cooper, A computer model for estimating the response of sprinkler links to compartment fires with draft curtains and fusible link-actuated ceiling vents, *Fire Technol.* **27**, 113–127 (1991).

APPENDIX: SOLVING THE PROBLEM FOR THE SPRAY CONE ENVELOPE

This appendix presents a procedure for numerical integration of equations (31)–(38). This is summarized in the Fig. 4 flow diagram of ref. [2].

The solution near elevations where $u_s^* = 0$

When the equations are integrated, special care is required since, per equations (31), Λ_3 and Λ_2, and therefore some of the right sides of equations (31)–(35), are singular at elevations where $u_s^* = 0$. Per equation (38), $x^* = x_w^*$ is always such an elevation. Other such elevations will occur for COND 4 or 5, at the elevations of jet penetration depth, $x^* = x_\delta^*$. Solution variables do indeed exhibit singular behavior at such elevations, the most significant involving a jump in T_s^* from its computed value immediately above the x_δ^* elevation, i.e. at $x^* = x_\delta^{*-}$, to the value $T_s^* = T_{LAYER}^*$ immediately below the x_δ^* elevation, i.e. at $x^* = x_\delta^{*+}$. As suggested earlier, the problem near $x^* = x_\delta^*$ and for $x^* \geqslant x_\delta^*$ can be treated in a manner which is completely analogous to the problem near $x^* = x_w^*$ and for $x^* \geqslant x_w^*$, respectively.

The solution near $x^* = x_w^*$

Analysis reveals that the singularity at $x^* = x_w^*$ is removable. Near $x^* = x_w^*$ the u_p^*, T_s^*, β, and $\dot{Q}_\delta^*$ are approximated by their initial values, 1, T_{LAYER}^*, 0, and 0, respectively, and u_s^* is:

$$\lim_{x^* \to x_w^*} u_s^* = [2\omega_3 T_{LAYER}^{*1/2}(T_{LAYER}^* + 1.55)^{0.35}/ x_x^{*2}]^{1/2}(x^* - x_w^*)^{1/2} + o(x^* - x_w^*)^{1/2}. \quad \text{(A1)}$$

Continuing the solution to arbitrary x^*

For specified small $\varepsilon > 0$, equation (A1) is used to estimate the solution from $x^* = x_w^*$ to $x^* = x_w^* + \varepsilon$. For $x^* > x_w^* + \varepsilon$, the solution would be obtained directly from numerical integrations of equations (31)–(35). The integrations would be continued to the smaller of following x^*s: $x^* = x_{FLOOR}^*$, at the floor, or $x^* = x_\delta^*$, at an elevation where $u_s^* \to 0$. If a $x_\delta^* < x_{FLOOR}^*$ value is identified, the solution would then be continued by appropriately re-initializing the problem at $x^* = x_\delta^*$ and integrating the equation set to $x^* = x_{FLOOR}^*$.

COND 1 scenarios are identified from the sprinkler–layer geometry. For this, integrations are carried out to $x^* = x_{FLOOR}^*$ without special considerations.

For COND 2–6 scenarios, integration is carried out to the interface, at $x^* = x_{INT}^*$, again with no special considerations. When equation (32) is satisfied at x_{INT}^{*+} a COND 3 or 4 scenario is indicated. When equation (32) is not satisfied at x_{INT}^{*+} a COND 2, 5, or 6 scenario is indicated. The remainder of this section will establish solution procedures for COND 2–6 scenarios.

COND 2–6 scenarios: identifying $x_\delta^* < x_{FLOOR}^*$; *solutions for* $x_{INT}^* < x^* \leqslant x_{FLOOR}^*$

General considerations. For a possible COND 2–6 scenario, it is not known *a priori* whether a value $x_\delta^* < x_{FLOOR}^*$ exists (i.e. COND 4 or 5). Furthermore, if such a x_δ^* does exist the solution for T_s^* is discontinuous at x_δ^*. During integration it

is required that the procedure be capable of determining x_δ^* and all solutions of the unknown variables to any specified accuracy. The solution strategy adopted here depends on the following observation: Assume that there is an $x_M^* < x_{FLOOR}^*$, where equation (32) is first satisfied and that integration of equations (32)–(35) from x_{INT}^* resulted in the identification of this elevation. Then it can be shown that $du_s^*/dx^* < 0$ uniformly in the range $x_M^* < x^* \leqslant x_\delta^*$ if $x_\delta^* < x_{FLOOR}^*$ exists, or in the range $x_M^* < x^* \leqslant x_{FLOOR}^*$ if $x_\delta^* < x_{FLOOR}^*$ does not exist. Accordingly, because u_s^* decreases monotonically with increasing x^* it is generally possible to continue the solution in a range which includes the possible singular elevation x_δ^* by exchanging dependent and independent variables x^* and u_s^* and integrating the revised equation set from $u_s^* = u_s^*(x_M^*)$ to $u_s^* = 0$. The revised equation set [only used if equation (32) is satisfied], which replaces equations (34) and (35) is:

$$\begin{aligned} dx^*/du_s^* &= 1/[-u_s^*/x^* + \Lambda_3 + \Lambda_4 - (\sigma/2)\Lambda_5] \\ dT_s^*/du_s^* &= -(T_s^*/u_p^*)\Lambda_5(du^*/du_s^*) \\ du_p^*/du_s^* &= (\Lambda_1 - \Lambda_2)(dx^*/du_s^*) \\ d\dot{Q}_d^*/du_s^* &= -\Lambda_5 x^{*2}(dx^*/du_s^*). \end{aligned} \tag{A2}$$

If an $x^*(u_s^*) > x_{FLOOR}^*$ is identified during the integration, then $u_s^* = 0$ above x_{FLOOR}^* cannot exist. Under such a circumstance no $x_\delta^* < x_{FLOOR}^*$ is possible, and the original equation set is integrated again from x_{INT}^* to x_{FLOOR}^*. Since it is now known that no singular x_δ^* value exists in this range, the latter integration will proceed to the end without difficulty.

If integration of the revised equation set is completed and $x^*(u_s^* = 0) < x_{FLOOR}^*$, then $x_\delta^* \equiv x^*(u_s^* = 0)$ and values of all variables at $u_s^* = 0$ are identified as the values of these variables at x_δ^{*-}. When this occurs, integration of the original equation set is continued from x_δ^{*+} to x_{FLOOR}^*. Since it is now known that no singular x_δ^* value exists in this latter range, the integration with appropriate initial conditions will proceed without difficulty and the solution can be completed. Further discussion on this final stage of integration is discussed below.

COND 2, 5, or 6 scenarios. If equation (32) is not satisfied at x_{INT}^*, COND 2, 5, or 6 is indicated and integration of the original equation set is continued from x_{INT}^* to x_{FLOOR}^*. At an intermediate stage of this latter integration an x_M^* elevation that may exist would be identified. If an x_M^* is not identified, a COND 6 scenario is indicated and the solution is completed.

If the integration reveals the existence and the value of an $x_M^* < x_{FLOOR}^*$, COND 2 or 5 scenario is indicated. Then integration of the original equation set is stopped at the x_M^* and the values of all variables there are identified. Integration with the revised equation set, equations (A2), is then continued from x_M^*. Finally, in accordance with the ideas outlined above, the integration proceeds to $x^* = x_{FLOOR}^*$ and the solution to the problem is completed.

COND 3 or 4 scenarios. If equation (33) is satisfied at x_{INT}^*, COND 3 or 4 is indicated and x_{INT}^* is identical to the x_M^* elevation. Integration of the problem with the revised equation set, equations (A2), is then initiated where the integration proceeds to $x^* = x_{FLOOR}^*$.

The solution for $x^* > x_\delta^*$

For COND 4 or 5 and for $x^* > x_\delta^*$, the above-indicated solution is obtained by solving a new initial value problem which involves the original equation set. The variables u_p^*, u_s^*, and $\dot{Q}_d^*$ are initialized at their previously-computed $x^* = x_\delta^{*-}$ values and the variable T_s^* is initialized at the value T_{LAYER}^*. According to the above definition of x_δ^* note that $u_s^*(x_\delta^{*-}) = 0$.

The equations have a singularity at $x^* = x_\delta^*$. As with the $x^* = x_w^*$ singularity, this one is also removable. Thus, near $x^* = x_\delta^*$, u_p^* and $\dot{Q}_d^*$ are approximated by their values at $x^* = x_\delta^{*-}$; T_s^* and β are assigned the values T_{LAYER}^* and 0, respectively; and the value of u_s^* is given by:

$$\lim_{x^* \to x_\delta^*} u_s^* = [2\omega_3 T_{LAYER}^{*1/2}(T_{LAYER}^* + 1.55)^{0.35} u_p^*(x_\delta^*)^{1/2}/ x_\delta^{*2}]^{1/2}(x^* - x_\delta^*)^{1/2} + o(x^* - x_\delta^*)^{1/2}. \tag{A3}$$

For a specified small $\varepsilon > 0$, the above values would be used to estimate the solution from $x^* = x_\delta^*$ to $x^* = x_\delta^* + \varepsilon$. For $x_\delta^* + \varepsilon < x^* \leqslant x_{FLOOR}^*$, this is obtained from equations (A2). No new singularities are possible and the indicated integration would proceed without difficulty.

INTERNATIONAL JOURNAL OF HEAT AND MASS TRANSFER
Volume 38, *No.* 4 *March* 1995

CONTENTS

(*Continued on inside back cover*)

Printed in Great Britain at BPC-AUP Aberdeen Ltd